Supporting Information:

Microscopic Theory of Resistive Switching in Ordered Insulators: Electronic vs. Thermal Mechanism

Jiajun Li[1], Camille Aron[2,3], Gabriel Kotliar[4] and Jong E. Han[1,*]

[1] *Department of Physics, State University of New York at Buffalo, Buffalo New York 14260, USA*

[2] *Laboratoire de Physique Théorique, École Normale Supérieure, CNRS PSL Research University, Sorbonne Universités, 75005 Paris, France*

[3] *Instituut voor Theoretische Fysica, KU Leuven, Belgium*

[4] *Department of Physics, Rutgers University, New Jersey 08854, USA*

[*]corresponding author e-mail:`jonghan@buffalo.edu`

I. CURRENT AND CURRENT LEAK TO THE FERMION RESERVOIRS

The steady-state electric current between nearest neighbor sites $\boldsymbol{r}$ and $\boldsymbol{r}+\hat{\boldsymbol{e}}$ is evaluated as

$$I_{\boldsymbol{r},\hat{\boldsymbol{e}}} = -\mathrm{i}t\sum_{\sigma}(\langle d^{\dagger}_{\boldsymbol{r}+\hat{\boldsymbol{e}}\sigma}d_{\boldsymbol{r}\sigma}\rangle - \mathrm{H.c.}) = -t\sum_{\sigma}\int\left[G^{<}_{\boldsymbol{r}+\hat{\boldsymbol{e}},\boldsymbol{r}}(\omega) - G^{<}_{\boldsymbol{r},\boldsymbol{r}+\hat{\boldsymbol{e}}}(\omega)\right]\frac{\mathrm{d}\omega}{2\pi}. \tag{1}$$

where the lesser Green's functions $G^{<}_{\boldsymbol{r}\boldsymbol{r}'}(\omega)$ are expressed in Eq. (7).

While the role the two leads is to supply both particle and heat transfer to/from the sample, the purpose of the local fermion reservoirs is to provide energy relaxation only. A uniform steady-state current in an infinite homogeneous lattice does not yield any particle flux to the fermion reservoirs that constitute the thermostats when their chemical potential is set to $\mu_{\boldsymbol{r}} = \varphi(\boldsymbol{r})$ [3]. However, in a finite or disordered lattice with a non-uniform current there can be a small volumic leakage of particles to the reservoirs, which can be expressed as

$$I_{\mathrm{leak},\sigma\boldsymbol{r}} = -\mathrm{i}\sum_{\alpha\sigma} g_{\boldsymbol{r}}(\langle d^{\dagger}_{\boldsymbol{r}\sigma}c_{\boldsymbol{r}\alpha\sigma}\rangle - \mathrm{H.c.}) = 2\Gamma_{\boldsymbol{r}}\int \mathrm{d}\omega\, A_{\sigma\boldsymbol{r}}(\omega)[f_{\sigma\boldsymbol{r}}(\omega) - f_0(\omega-\mu_{\boldsymbol{r}})]\,, \tag{2}$$

with the local density of states $A_{\sigma\boldsymbol{r}}(\omega) = -\pi^{-1}\mathrm{Im}\, G^{\mathrm{R}}_{\sigma}(\omega)_{\boldsymbol{r}\boldsymbol{r}}$ and the local nonequilibrium distribution function $f_{\sigma\boldsymbol{r}}(\omega) = G^{<}_{\sigma}(\omega)_{\boldsymbol{r}\boldsymbol{r}}/(2\pi\mathrm{i}A_{\sigma\boldsymbol{r}}(\omega))$. Therefore, we slightly adjust the local chemical potential $\mu_{\boldsymbol{r}}$ at each HF iteration to ensure the vanishing of $I_{\mathrm{leak},\sigma\boldsymbol{r}}$ and prevent any particle leak.

II. NEGATIVE DIFFERENTIAL RESISTANCE SOLUTION VIA EXTERNAL RESISTOR

In this Section, we explain the relations between $I(V_{\mathrm{t}})$ in FIG. 3(a) and $I(V_{\mathrm{s}})$ in FIG. 3(b) of the Letter, and how to access the negative differential resistance (NDR) regime of the latter.

In FIG. 3(a), the current is plotted as a function of the total voltage imposed by the dc generator on the circuit, V_{t}. $I(V_{\mathrm{t}})$ corresponds to what is directly measured in experiments. However, in order to characterize a sample independently of the details of the external electrical circuit, one is interested in giving the current versus the voltage drop across the sample, V_{s}. $I(V_{\mathrm{s}})$ is the *intrinsic* characteristic of the sample, plotted in FIG. 3(b).

While both $I(V_{\mathrm{s}})$ and $I(V_{\mathrm{t}})$ are of course trivially related to one-another by Kirchhoff's laws, which in our case simply yield

$$V_{\mathrm{t}} = V_{\mathrm{s}} + RI\,, \tag{3}$$

the measurement of $I(V_{\mathrm{t}})$ for all V_{t} does not guaranty the full knowledge of $I(V_{\mathrm{s}})$. Indeed, if the latter is non-monotonous or multivalued, parts of the $I(V_{\mathrm{s}})$ characteristic will be inaccessible, *i.e.* hidden, unless the external resistance is selected with care [5].

To illustrate this point, let us re-write Eq. (3) as

$$\frac{V_{\mathrm{t}} - V_{\mathrm{s}}}{R} = I(V_{\mathrm{s}}). \tag{4}$$

This expresses that fact that for a given V_{t} delivered by the dc generator, both I and V_{s} are self-consistent solutions that live at the intersection(s) of the line $(V_{\mathrm{t}} - V_{\mathrm{s}})/R$ (LHS) with the characteristic $I(V_{\mathrm{s}})$ (RHS).

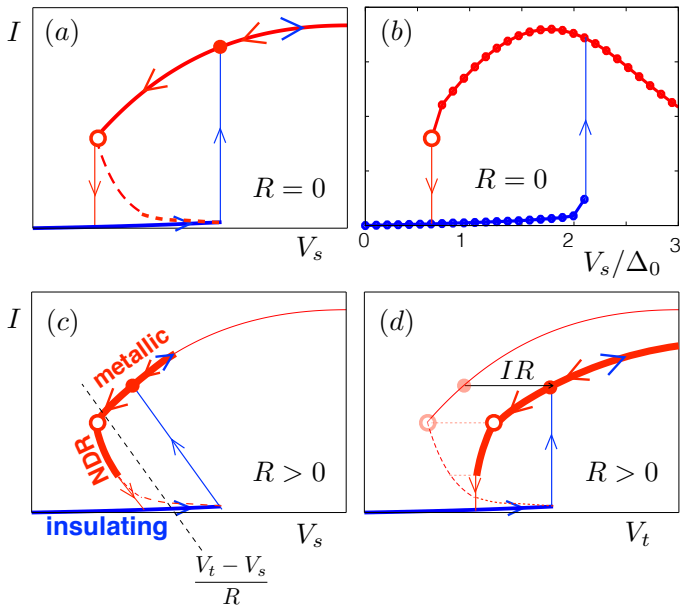

Figure S1: (a) Schematic I-V plot with zero external resistance $R = 0$ and (b) the actual numerical results ($c = 0.03$). Schematic graphs (c) plotted against the sample voltage V_s with $R > 0$ and (d) plotted against the total voltage V_t with $R > 0$. The blue (resp. red) arrows denote the solutions obtained when increasing (resp. decreasing) the total voltage V_t. White circles mark the first appearance of insulating regions on the edges of the metallic sample when decreasing V_t on the metallic branch.

In our case, we are dealing with S-shaped $I(V_\mathrm{s})$ characteristics, for which the current happens to be multivalued for given values of the voltage, see the sketch in FIG. S1(a). Another case, which we shall not examine here, are N-shaped $I(V_\mathrm{s})$ characteristics for which it is the voltage that is multivalued for a given current. In our case, the physical reason behind that peculiar S shape is the appearance (see the white circles in FIG. S1) and the rapid growth of insulating domains when reducing the voltage bias ahead of the MIT, as shown in FIG. 5(a-b) of manuscript. This causes an NDR regime, $\mathrm{d}I/\mathrm{d}V_\mathrm{s} < 0$, which extends until the sample is fully metallic. For the discussion, we decompose the $I(V_\mathrm{s})$ characteristic in three branches: the insulating branch, the metallic branch, and the NDR branch in the middle, see FIG. S1(a).

To understand why the NDR branch of the $I(V_\mathrm{s})$ characteristic needs extra care to be revealed, let us first consider the case $R = 0$ illustrated schematically in FIG. S1(a) and computed numerically in FIG. S1(b). At $V_\mathrm{t} = 0$, there is a single trivial solution: $I = 0$ and $V_\mathrm{s} = 0$. As V_t is slowly increased, the solution remains by continuity on the insulating branch of the $I(V_\mathrm{s})$ characteristic, even when two extra solutions have appeared on the other branches of the S. For larger voltages, when $V_\mathrm{t} = V_\mathrm{IMT}$, the insulating branch stops, and the current makes a brutal and discontinuous transition towards the solution on the metallic branch. As V_t is now slowly decreased, the systems remains on the metallic branch, until it stops at $V_\mathrm{t} = V_\mathrm{MIT}$, where the current jumps back on the insulating branch. We see that without external resistance, $R = 0$, the system experiences a strong hysteresis making it impossible to probe the NDR branch of the $I(V_\mathrm{s})$ characteristic, no matter the value of V_t

It is not hard to show that the condition on the resistance to avoid any hysteresis loop, and

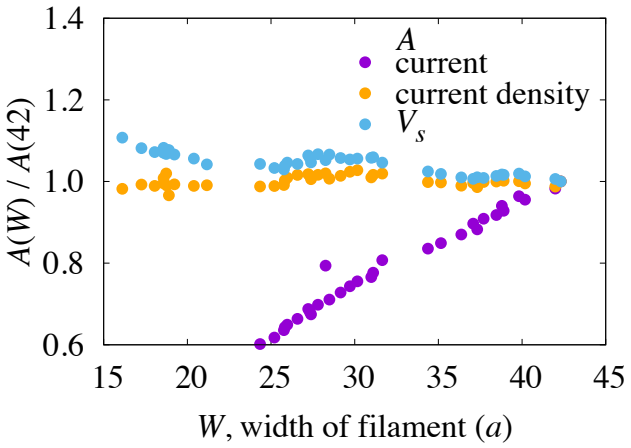

Figure S2: Current and sample voltage V_s as a function of the filament width W on the negative-differential-conductance branch. Inside the filament, the electric current density (measured and averaged alng the central line of the filament) is nearly independent of W while the voltage slightly increases as the width decreases.

therefore probe the full NDR branch, is

$$R > R_\mathrm{min} \text{ with } \frac{1}{R_\mathrm{min}} \equiv \min\left\{\left|\frac{\mathrm{d}I(V_\mathrm{s})}{\mathrm{d}V_\mathrm{s}}\right| ; V_\mathrm{s} \in [V_\mathrm{MIT}, V_\mathrm{IMT}]\right\} , \tag{5}$$

which guaranties a unique solution to Eq. (4) for all values of V_t. This is particularly clear in the limit $R \to \infty$, where the LHS of Eq. (4) is an horizontal line, always intersecting $I(V_\mathrm{s})$ at a single point. Such a current-controlled measurement has been performed experimentally in Ref. [6], where the NDR branch was thereby fully uncovered.

In the intermediate cases, $0 < R < R_\mathrm{min}$, the NDR branch can only be partially revealed, as shown in FIG. S1(c). This is the case for the numerical data presented in the manuscript (the external resistance was set to $R = 0.634$).

III. NEGATIVE DIFFERENTIAL RESISTANCE MECHANISM

The NDR in the resistive switching is characterized by the metal-insulator coexistent phase. The main experimental observation is that the I-V curve is very steep [6, 7] with the slope $|\mathrm{d}I/\mathrm{d}V_\mathrm{s}|$ decreasing with increasing sample bias V_s, which was reproduced by the calculation in the main text. The mechanism for the NDR can be understood as follows. As shown in Figure S2, the current density inside the filament is the property of the bulk metallic state and remains nearly constant as a function of the filament width W. Therefore, the total current is linearly proportional to W, as clearly shown in the figure. On the other hand, the voltage drop in the sample is given by the *resistivity* of the metallic state and current density, with the *resistance* being nearly independent of the current, leading to a vertical I-V relation. However, as indicated by the data in the figure, the voltage drop slightly increases at small W, due to the enhanced scattering from domain boundaries of the filament. This opposite behavior of I and V as a function of the filament width is the origin of the NDR. For instance, an increase of current is mainly due to the growing filament width, which results in less electron scattering and reduced resistance and voltage drop across the sample.

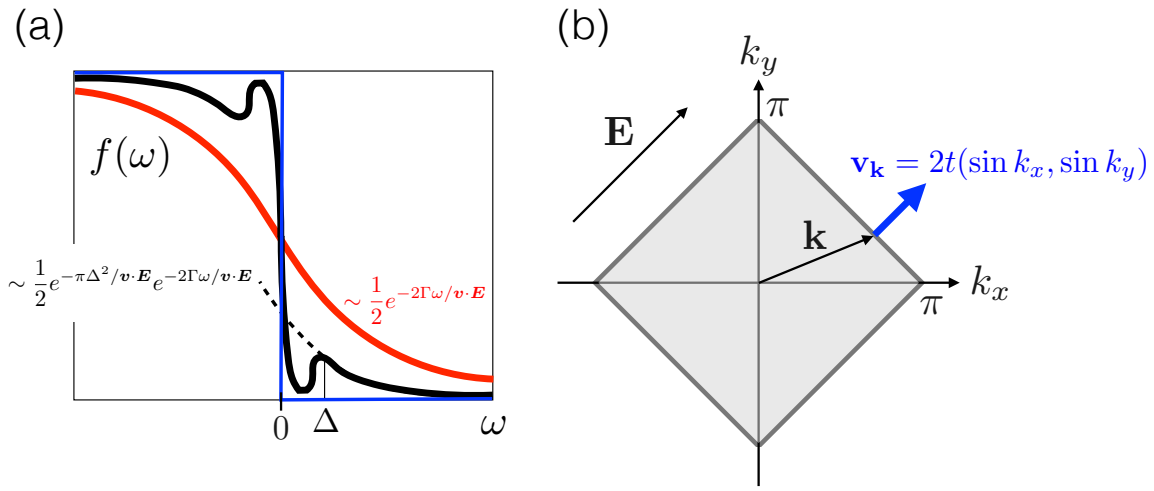

Figure S3: (a) Schematic plot of the local energy distribution function given in FIG. 1 of the Letter. The metallic distribution (red), with a tail $\sim \frac{1}{2}\mathrm{e}^{-\Gamma\omega/vE}$, is reduced in the gapped phase (black) by the Landau-Zener factor $\mathrm{e}^{-\pi\Delta^2/\boldsymbol{v}\cdot\boldsymbol{E}}$ as outlined by the dashed line that fits most of the nonequilibrium energy distribution. The equilibrium distribution (blue) at $E = 0$ is a step function because the environment is kept at zero temperature. (b) Fermi sea of a $2d$ square lattice at half-filling. The electric field $\mathbf{E}$ is oriented along the $(1, 1)$ direction, as in FIG. 1 of the Letter.

This demonstrates that the NDR in the RS is an *intrinsic* property of the sample, independent of the external resistor. The external resistor only helps the algorithm to find the NDR branch out of the three possible stable solutions for E-field with $E_{\mathrm{MIT}} < E < E_{\mathrm{IMT}}$. We can numerically prove that the NDR is an intrinsic property of the sample, as follows. We proceed as in Figure S1(c) from the metallic branch by decreasing the total voltage V_{t}, and stop the simulation as soon as the NDR solution is found, right past the white circle. We then remove the external resistor from the circuit and increase the voltage which is now the sample voltage V_{s}. This procedure reproduces the same NDR I-V relation as shown in Figure S1(c). This behavior was confirmed on the curves reported on the main text.

IV. ENERGY DISTRIBUTION FUNCTION

In this Section, we discuss the local energy distribution function which provides valuable quantum mechanical information about the nonequilibrium dynamics. It is defined as

$$f_{\boldsymbol{r}}(\omega) = -\frac{1}{2}\frac{\mathrm{Im}G^{<}_{\sigma}(\omega)_{\boldsymbol{rr}}}{\mathrm{Im}G^{\mathrm{R}}_{\sigma}(\omega)_{\boldsymbol{rr}}}. \tag{6}$$

and reduces to the Fermi-Dirac function in equilibrium ($E = 0$). Within the HF approximation, the lesser Green's function can be expressed as [3]

$$G^{<}_{\boldsymbol{rr'}}(\omega) = 2\mathrm{i}\Gamma\sum_{\boldsymbol{r''}} G^{\mathrm{R}}_{\boldsymbol{rr''}}(\omega)[G^{\mathrm{R}}_{\boldsymbol{r''r'}}(\omega)]^{*} f_0(\omega + \boldsymbol{r''}\cdot\boldsymbol{E}), \tag{7}$$

and locally, we have

$$G^{<}_{\boldsymbol{00}}(\omega) = 2\mathrm{i}\Gamma\sum_{\boldsymbol{r}} |G^{\mathrm{R}}_{\boldsymbol{0r}}(\omega)|^2 f_0(\omega + \boldsymbol{r}\cdot\boldsymbol{E}), \tag{8}$$

where $f_0(\omega)$ is the Fermi-Dirac distribution of the fermion reservoirs maintained in equilibrium at temperature $T_{\rm bath}$. In the case of a pure metal (non-interacting limit), it was already shown in Ref. [3] that the precise shape of the nonequilibrium distribution function is the result of superimposing the Fermi-Dirac distributions originating from the fermion reservoirs at distant sites with chemical potential governed by the bias potential $\varphi(\boldsymbol{r})$. It is the overall profile of the resulting nonequilibrium distribution that can be used to define an effective temperature $T_{\rm eff}$, *a priori* much different from $T_{\rm bath}$. See, for example, FIG. S2(a) where the driven metallic phase (in red) displays a hot $T_{\rm eff}$. We shall discuss this effective temperature in more details in Sect. V. Noteworthy, one can interpret the above factor $|G^{\rm R}_{\mathbf{0}\boldsymbol{r}}(\omega)|^2$, which is the wavefunction overlap between sites $\boldsymbol{r}$ and $\mathbf{0}$ due to quantum tunneling, as the coupling strength of the statistical information across the lattice. We emphasize that this nonequilibrium distribution is the result of electronic processes only. Therefore, it should establish itself much faster than a simple thermal diffusion process.

The above formal discussion on the electronic origin of the nonequilibrium distribution function can be corroborated by showing explicitly that the nonequilibrium excitations correspond to Landau-Zener tunneling processes (LZT) [9] over the gap Δ. If this claim is correct, it implies that the nonequilibrium distribution functions of the metallic phase (where $\Delta = 0$) and the insulating phase (where $\Delta > 0$) mostly differ by a LZT factor $\mathrm{e}^{-\pi\Delta^2/|\boldsymbol{v}\cdot\boldsymbol{E}|}$, as depicted schematically in FIG. S2(a). To test this claim, we compare the numerical results with the LZT predictions on the total number of nonequilibrium excitations above the chemical potential,

$$P_{\rm ex}(\Delta) = \int_0^\infty A(\omega;\Delta) f(\omega;\Delta) \mathrm{d}\omega \,, \tag{9}$$

where $A(\omega) = -\pi^{-1}\mathrm{Im}G^R_{\rm loc}(\omega)$ is the local density of states. On the one hand, we compute Eq. (9) numerically. On the other hand, we estimate $P_{\rm ex}(\Delta)$ as the steady-state number of excitations in the presence of two competing processes: LZT events occurring at a rate $\gamma_{\rm LZ}(\Delta) \sim E \exp\left(-\pi\Delta^2/|\boldsymbol{v}_{\boldsymbol{k}}\cdot\boldsymbol{E}|\right)$ (the precise numerical prefactor arises from the Bloch oscillations frequency), and relaxation events occurring at a rate $\sim \Gamma$. We therefore obtain, summed over the Fermi surface (FS),

$$P_{\rm ex}(\Delta) = \frac{1}{\mathcal{S}_{\rm FS}} \int_{\boldsymbol{k}\in{\rm FS}} \mathrm{d}\boldsymbol{k} \; \frac{\gamma_{LZ}(\Delta)}{\gamma_{LZ}(\Delta)+\Gamma} \,, \tag{10}$$

where $\mathcal{S}_{\rm FS}$ is the Fermi surface area. In our case of a $2d$ square lattice with the field $\boldsymbol{E}$ along the $(1,1)$ diagonal, the group velocity at the half-filled Fermi surface is either parallel or perpendicular to $\boldsymbol{E}$. We can therefore reduce the Fermi surface integral to its first quadrant defined as $k_x + k_y = \pi$ [see Fig. S2(b)], yielding the prediction

$$P_{\rm ex}(\Delta) = \frac{1}{\pi}\int_0^\pi \mathrm{d}k_x \frac{\frac{E}{\sqrt{2}}\exp\left(-\frac{\pi\Delta^2}{2\sqrt{2}tE\sin k_x}\right)}{\frac{E}{\sqrt{2}}\exp\left(-\frac{\pi\Delta^2}{2\sqrt{2}tE\sin k_x}\right)+\Gamma} \,. \tag{11}$$

In FIG. 1(d) of the Letter, we compare this LZT prediction with the numerics. They display an excellent agreement over several orders of magnitude of the gap Δ. This demonstrates that the Landau-Zener tunneling is responsible for the nonequilibrium excitations.

V. EFFECTIVE TEMPERATURE

In this Section, we discuss and justify the expression for the effective temperature

$$T_{\rm eff} \sim \frac{|\boldsymbol{E}\cdot\boldsymbol{v}_{\rm F}|}{\Gamma}\,, \tag{12}$$

which we use inside metallic domains to argue for the strong dependence of Joule heating on the crystallographic direction with respect to the field direction. Aside from this geometric consideration, note that this expression also transparently elucidated how Joule heating sets the temperature as the result of a balance between the drive $\boldsymbol{E}$ and the energy relaxation rate Γ.

In the metallic regime, we can start by neglecting the on-site Coulomb interaction. Within a first-order gradient approximation, *i.e.* when the spatial and temporal inhomogeneities of the system occur on mesoscopic scales, the Quantum Boltzmann Equation governing the distribution function f_σ reads, dropping the spin index,

$$\left[\partial_T + \boldsymbol{v}(\boldsymbol{k})\cdot\boldsymbol{\nabla}_{\boldsymbol{X}} + \boldsymbol{E}\cdot\boldsymbol{\nabla}_{\boldsymbol{k}}\right] f(X;k) = 2\Gamma\left[f_0(\omega-\mu_{\boldsymbol{X}}) - f(X;k)\right]\,. \tag{13}$$

Here, $X=(T,\boldsymbol{X})$ are space-time coordinates and $k=(\omega,\boldsymbol{k})$ are Fourier components. The velocity is given by $\boldsymbol{v}(\boldsymbol{k})=\boldsymbol{\nabla}_{\boldsymbol{k}}\epsilon(\boldsymbol{k})$ where $\epsilon(\boldsymbol{k})$ is the dispersion relation (square lattice in our case). Having neglected the Coulomb interactions, the collision integral on the RHS is only due to the scattering with the degrees of freedom of the local thermostats in equilibrium at temperature $T_{\rm bath}$ and chemical potential $\mu_{\boldsymbol{X}}=-\boldsymbol{E}\cdot\boldsymbol{X}$. $f_0(\epsilon)\equiv[1+\exp(\epsilon/T_{\rm bath})]^{-1}$ is the Fermi-Dirac distribution. Once a steady state is reached, it simplifies to

$$\left[\boldsymbol{v}(\boldsymbol{k})\cdot\boldsymbol{\nabla}_{\boldsymbol{X}} + \boldsymbol{E}\cdot\boldsymbol{\nabla}_{\boldsymbol{k}}\right] f(X;k) = 2\Gamma\left[f_0(\omega+\boldsymbol{E}\cdot\boldsymbol{X}) - f(X;k)\right]\,. \tag{14}$$

If analyzing this equation order by order in $\boldsymbol{E}$, *i.e.* decomposing $f(\boldsymbol{X};k)=f_0(\omega)+\boldsymbol{E}\cdot\boldsymbol{f}^{(1)}+E_iE_j\,f^{(2)}_{ij}+\ldots$, one can check that the contribution from the term in $\boldsymbol{E}\cdot\boldsymbol{\nabla}_{\boldsymbol{k}}$ in Eq. (14) is of higher order than those of the other terms and can therefore be neglected in a first approximation. Therefore we simplify further the equation to work with

$$\boldsymbol{v}(\boldsymbol{k})\cdot\boldsymbol{\nabla}_{\boldsymbol{X}} f(X;k) = 2\Gamma\left[f_0(\omega+\boldsymbol{E}\cdot\boldsymbol{X}) - f(X;k)\right]\,. \tag{15}$$

In the limit of zero-temperature thermostats, $T_{\rm bath}\to 0$, we obtain the following solution

$$\begin{aligned} f(\boldsymbol{X};\omega,\boldsymbol{k}) &= \Theta(-\omega-\boldsymbol{E}\cdot\boldsymbol{X}) \\ &\quad + \frac{1}{2}\left[\mathrm{sign}(\omega+\boldsymbol{E}\cdot\boldsymbol{X}) + \mathrm{sign}\left(\boldsymbol{E}\cdot\boldsymbol{v}(\boldsymbol{k})\right)\right]\exp\left(-2\Gamma\left|\frac{\omega+\boldsymbol{E}\cdot\boldsymbol{X}}{\boldsymbol{E}\cdot\boldsymbol{v}(\boldsymbol{k})}\right|\right)\,. \end{aligned} \tag{16}$$

where $\Theta(\epsilon)$ is the Heaviside step function. For wave-vectors $\boldsymbol{k}^*$ such that $\boldsymbol{E}\perp\boldsymbol{v}(\boldsymbol{k}^*)$, this simplifies to

$$f(\boldsymbol{X};\omega,\boldsymbol{k}^*) = \Theta(-\omega-\boldsymbol{E}\cdot\boldsymbol{X})\,, \tag{17}$$

which is the zero-temperature Fermi-Dirac distribution, $\lim_{T_{\rm bath}\to 0} f_0(\omega-\mu_{\boldsymbol{X}})$. On the contrary, for wave vectors such that $\boldsymbol{v}(\boldsymbol{k})$ is parallel to the local $\boldsymbol{E}$ field, the distribution is far from the zero-temperature equilibrium of the thermostats. One can extract an effective temperature from the solution expressed in Eq. (16), $T_{\rm eff}(\boldsymbol{k})\sim|\boldsymbol{E}\cdot\boldsymbol{v}(\boldsymbol{k})|/\Gamma$, which depends on $\boldsymbol{k}$. In a

non-interacting metal, and in the weak-field limit, electrons traveling in the direction of the electric field are "hotter" than those traveling perpendicularly. Altogether, given that the electrons contributing most to transport are those at the Fermi surface, with velocity $\boldsymbol{v}_{\mathrm{F}}$, we identify the effective temperature

$$T_{\mathrm{eff}} \sim \frac{|\boldsymbol{E} \cdot \boldsymbol{v}_{\mathrm{F}}|}{\Gamma} \,. \tag{18}$$

This expression can be approximately generalized to include corrections from the Coulomb interactions by renormalizing the bare electric field with Hartree-Fock corrections, $\boldsymbol{E} \to \tilde{\boldsymbol{E}}_\sigma(\boldsymbol{X}) \equiv \boldsymbol{E} - \boldsymbol{\nabla}_{\boldsymbol{X}} \left[U \langle n_{-\sigma}(\boldsymbol{X}) \rangle\right]$, yielding in particular a dependence on the inhomogeneities of the non-equilibrium charge distribution.

---

[1] N. Tsuji, T. Oka, and H. Aoki, Phys. Rev. B **78**, 235124 (2008).
[2] C. Aron, G. Kotliar, and C. Weber, Phys. Rev. Lett. **108**, 086401(2012).
[3] J. E. Han and J. Li, Phys. Rev. B **88**, 075113 (2013).
[4] J. Li, C. Aron, G. Kotliar, and J. E. Han, Phys. Rev. Lett. **114**, 226403 (2015).
[5] B. K. Ridley, Proc. Phys. Soc. **82**, 954 (1963).
[6] H.-T. Kim, B.-J. Kim, S. Choi, B.-G. Chae, Y. W. Lee, T. Driscoll, M. M. Qazilbash, and D. N. Basov, J. Appl. Phys. **107**, 023702 (2010).
[7] A. Zimmers, L. Aigouy, M. Mortier, A. Sharoni, S. Wang, K. G. West, J. G. Ramirez, and I. K. Schuller, Phys. Rev. Lett. **110**, 056601 (2013).
[8] E. Janod, J. Tranchant, B. Corraze, M. Querré, P. Stoliar, M. Rozenberg, T. Cren, D. Roditchev, V. Ta Phuoc, M.-P. Besland, and L. Cario, Adv. Funct. Mater. **25** 6287 (2015).
[9] C. Zener, Proc. R. Soc. Lond. A **137**, 696 (1932).